

# Numerical evaluation of virtual corrections to multi-jet production in massless QCD

---

**Simon Badger<sup>a</sup> Benedikt Biedermann<sup>b</sup> Peter Uwer<sup>b</sup> Valery Yundin<sup>a</sup>**

<sup>a</sup>*Niels Bohr International Academy and Discovery Center, The Niels Bohr Institute,  
University of Copenhagen, Blegdamsvej 17, DK-2100 Copenhagen, Denmark*

<sup>b</sup>*Humboldt-Universität zu Berlin, Institut für Physik,  
Newtonstraße 15, D-12489 Berlin, Germany*

*E-mail:* [badger@nbi.dk](mailto:badger@nbi.dk), [benedikt.biedermann@physik.hu-berlin.de](mailto:benedikt.biedermann@physik.hu-berlin.de),  
[peter.uwer@physik.hu-berlin.de](mailto:peter.uwer@physik.hu-berlin.de), [yundin@nbi.dk](mailto:yundin@nbi.dk)

**ABSTRACT:** We present a C++ library for the numerical evaluation of one-loop virtual corrections to multi-jet production in massless QCD. The pure gluon primitive amplitudes are evaluated using NGLUON [1]. A generalized unitarity reduction algorithm is used to construct arbitrary multiplicity fermion-gluon primitive amplitudes. From these basic building blocks the one-loop contribution to the squared matrix element, summed over colour and helicities, is calculated. No approximation in colour is performed. While the primitive amplitudes are given for arbitrary multiplicities we provide the squared matrix elements only for up to 7 external partons allowing the evaluation of the five jet cross section at next-to-leading order accuracy. The library has been recently successfully applied to four jet production at next-to-leading order in QCD [2].

Draft from September 18, 2018

---

## Contents

<b>1</b>	<b>Introduction</b>	<b>1</b>
<b>2</b>	<b>Methods</b>	<b>2</b>
2.1	Multiple Fermion Primitive Amplitudes	2
2.2	Partial Amplitudes and Colour Summation	4
2.3	Cache system for tree amplitudes	8
2.4	Universal Pole Structure and Scheme Dependence	9
<b>3</b>	<b>Installation and Usage</b>	<b>10</b>
3.1	Interface via the Binoth Les Houches Accord	11
3.1.1	Additional BLHA options	12
3.2	The <code>NParton</code> library for multi-parton primitives	13
3.2.1	Initialization and Namespaces	13
3.2.2	Constructor	13
3.2.3	Member functions	13
<b>4</b>	<b>Results</b>	<b>15</b>
4.1	Validation	15
4.2	Accuracy	17
4.3	Speed Tests	17
<b>5</b>	<b>Conclusions</b>	<b>20</b>
<b>A</b>	<b>Numerical cross checks</b>	<b>21</b>
<b>B</b>	<b>Numerical evaluation for 7-parton virtual corrections</b>	<b>25</b>

---

## 1 Introduction

Next-to-leading order (NLO) corrections to multi-particle Standard Model processes at hadron colliders are essential for quantitative predictions of the large QCD background to many new physics scenarios.

Though the computation of the one-loop virtual corrections with four or more final state particles has always presented a theoretical challenge, new methods like unitarity [3, 4], generalized unitarity [5–8] and integrand reduction [9] have been developed into effective tools suited for a wide variety of processes. We also note that the traditional approach—the powerful work horse of the last three decades for perturbative calculations in quantum field theory—has been refined and improved continuously. For recent developments we refer for example to Ref. [10].

A number of automated approaches have been developed in the last five years [11–16] some of which are now publicly available. On-shell techniques have also been used recently to compute compact analytic matrix elements within the popular MCFM program [17–22]. The availability of one-loop corrections combined with real radiation contributions have made an increasingly large number of phenomenological studies possible [23–46]. More recently improvements beyond fixed-order in perturbation theory using parton shower matching techniques [47–49] have been achieved for a number of non-trivial cases [50–59]. Despite the tremendous progress there is still room for improvement in terms of efficiency and flexibility before one-loop computations reach the same level of automation as tree-level predictions and a number of interesting new directions continue to appear [10, 60, 61].

In this paper we present the C++ library NJET for the numerical evaluation of one-loop amplitudes for multi-jet production in massless QCD. The on-shell generalized unitarity algorithm employed in NJET is well suited to deal with the large amount of gluonic radiation which complicates a traditional Feynman approach to such processes. Our paper is organized as follows: first we briefly review the method of generalized unitarity used for the construction of primitive amplitudes with arbitrary numbers of fermion pairs. We then describe the construction of full colour and helicity summed squared amplitudes by partial amplitudes in terms of the computed primitive amplitudes. A detailed description of the installation procedure and the usage of the NJET package is presented in section 3 including a short summary of the interface via the Binoth Les Houches Accord (BLHA) [62]. In section 4 we discuss the validation of the NJET library. In particular we present cross checks with available analytic results and show a numerical comparison for selected benchmark points. In addition we present some performance tests of the program that investigate numerical accuracy and speed of both primitive and colour summed amplitudes.

## 2 Methods

The NJET library is built upon the framework of NGLUON [1] which uses generalized unitarity to construct primitive gluon amplitudes. This procedure allows one-loop amplitudes to be constructed from tree-level amplitudes via the solution to a system of cut equations. One important aspect of this method is that it maps the problem of computing any one-loop amplitude to the solution of a linear system of equations which is well suited for numerical evaluation. Furthermore the method uses on-shell amplitudes instead of individual Feynman diagrams avoiding the significant growth in complexity when one-loop amplitudes for large multiplicities are considered.

The implementation in NGLUON uses the algorithm of Ellis, Giele, Kunszt and Melnikov [6, 7] to construct the coefficients of the scalar one-loop integrals. For the rational terms we map the problem of cuts in  $4 - 2\epsilon$  dimensions to that of four dimensional massive cuts. The scalar one-loop integrals are all known analytically and are evaluated using the FF/QCDLoop package [63, 64]. An alternative implementation by van Hameren now allows for full complex masses and quadruple precision evaluation of the integral functions [65].

### 2.1 Multiple Fermion Primitive Amplitudes

A new feature added to the NGLUON package to enable the application to multi-jet production at NLO is the ability to compute primitive amplitudes with an arbitrary number of external and

internal quarks. First results have been presented recently in references [66, 67]. In the following we briefly comment on this extension of NGLUON.

An  $n$ -particle, one-loop primitive amplitude is defined by an ordered set of  $n$  external particles and a set of propagators specifying the loop content. These primitive amplitudes are gauge invariant sums of colour ordered Feynman diagrams as introduced in Ref. [68]. The full set of independent primitives falls into two subclasses:

- Amplitudes with a mixture of quark and gluon propagators,  $A_n^{[m]}$ ,
- Amplitudes with an internal fermion loop,  $A_n^{[f]}$ .

Each primitive amplitude can be associated uniquely with a “parent diagram” [69]. This is a diagram with  $n$  propagators and  $n$  colour ordered three-vertices from which all contributing ordered Feynman diagrams can be obtained by “pinching” and “pulling” operations. The parent diagrams of the two classes of primitives above are determined by the external legs and the parton type of the propagator appearing immediately before the first leg. All other internal parton types will then follow from the preceding ones, two examples of this are shown in Figure 1. In cases where the corresponding vertices do not exist and no internal propagator can be connected we attribute a special propagator as placeholder in order to ensure that the parent diagram always contains a total of  $n$  propagators.

Once the parent diagram of the primitive amplitude has been constructed the generalized unitarity algorithm can be applied to compute the coefficients of the scalar integral basis by factorizing each cut into a product of tree-level amplitudes. These amplitudes are then computed with off-shell Berends-Giele recursion relations [70]. With a suitable caching system for the off-shell currents, this approach scales polynomially in complexity at  $O(n^4)$  with  $n$  being the number of external legs. The power of four arises from the four-gluon vertex, which dominates the recursion for large  $n$ , independent on the number of quark pairs. The inclusion of fermions is rather a matter of book-keeping and no conceptual difficulties arise.

The rational terms are evaluated by using four-dimensional massive cuts to obtain  $D$ -dimensional cut information [71, 72]. This corresponds to working in the four-dimensional helicity (FDH) scheme [73] which is equivalent to dimensional reduction at one-loop. The coefficients of the  $D$ -dimensional integral basis [7] are efficiently extracted using a discrete Fourier projection on the

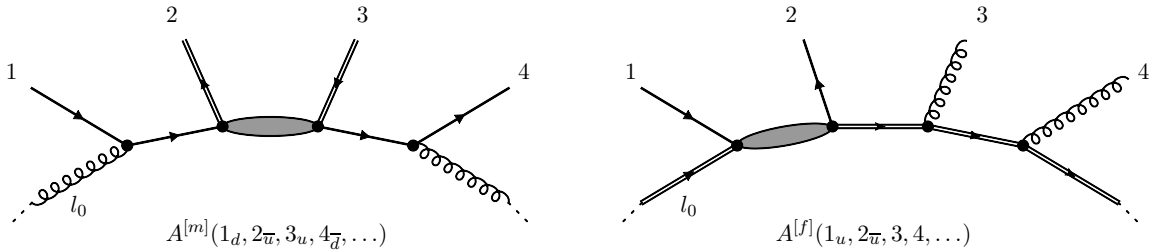


**Figure 1.** Constructing parent diagrams for the primitive amplitudes. In case that no internal propagator can be connected since the corresponding vertices do not exist a blank propagator is inserted, represented graphically as a shaded blob.

internal mass [74, 75]. When only concerned with the rational terms it is possible to replace all internal  $D$ -dimensional gluons with massive scalars and treat  $D$ -dimensional fermions with massive fermions. The computation of the rational term is therefore a direct copy of the extraction of the integral coefficients but with different tree-level amplitudes which are also straightforward to compute with off-shell recursion relations. In addition one can use supersymmetry identities [68] to find relations between the rational terms of the two classes of primitives  $A^{[m]}$  and  $A^{[f]}$  which allows for a more efficient construction of the full colour amplitudes. This has been implemented for fermion loops in both the pure gluon and single fermion pair amplitudes:

$$\mathcal{R}\left(A_n^{[m]}(1, \dots, n) - A_n^{[f]}(1, \dots, n)\right) = 0, \quad (2.1)$$

$$\begin{aligned} &\mathcal{R}\left(A_n^{[m]}(1_{\bar{q}}, 2, \dots, (k-1), k_q, (k+1), \dots, n) \right. \\ &+ (-1)^n A_n^{[m]}(1_{\bar{q}}, n, \dots, (k+1), k_q, (k-1), \dots, 2) \\ &- A_n^{[f]}(1_{\bar{q}}, 2, \dots, (k-1), k_q, (k+1), \dots, n) \\ &\left. - (-1)^n A_n^{[f]}(1_{\bar{q}}, n, \dots, (k+1), k_q, (k-1), \dots, 2)\right) = 0, \end{aligned} \quad (2.2)$$

where the operator  $\mathcal{R}$  denotes taking the rational part of the amplitude.

## 2.2 Partial Amplitudes and Colour Summation

To build the full colour amplitudes from the primitive one-loop amplitudes provided by NGLUON and its extension to massless quarks we must construct the coefficients of the  $SU(N_c)$  colour factors, the partial amplitudes. In general the full colour  $L$ -loop amplitude can be written as:

$$\mathcal{A}_n^{(L)}(\{p_i\}) = \sum_c T_c^{(L)}(\{a_i\}) A_{n;c}^{(L)}(p_1, \dots, p_n), \quad (2.3)$$

where  $A_{n;c}$  are the partial amplitudes and the summation is performed over all different colour structures  $T_c^{(L)}(\{a_i\})$  which depend on the colour of the external partons abbreviated here by  $a_i$ . For the evaluation of the colour summed squared matrix elements we construct colour matrices  $C$  by taking the product of colour structures and summing over the colour degrees of freedom of the external partons,

$$C_{cc'}^{(0)} = \sum_i T_c^{(0)}(\{a_i\}) \cdot T_{c'}^{(0)}(\{a_i\}), \quad (2.4)$$

$$C_{cc'}^{(1)} = \sum_i T_c^{(0)}(\{a_i\}) \cdot T_{c'}^{(1)}(\{a_i\}). \quad (2.5)$$

The colour summed squared Born amplitude will then be constructed from the tree-level partial amplitudes  $A_{n;c}^{(0)}$  according to

$$d\sigma^{LO} \sim A_{n;c}^{(0)\dagger} \cdot C_{cc'}^{(0)} \cdot A_{n;c'}^{(0)}. \quad (2.6)$$

The one-loop interference term is given in complete analogy by

$$d\sigma^{NLO} \sim A_{n;c}^{(0)\dagger} \cdot C_{cc'}^{(1)} \cdot A_{n;c'}^{(1)}. \quad (2.7)$$

The entries of the colour matrix are given in terms of products of  $SU(N_c)$  generators summed over colour indices which we evaluate directly into a rational function in  $N_c$  before hard coding the result into C++.

The algorithm for determining the decomposition of the partial amplitudes in terms of primitive amplitudes has been constructed along the lines of that suggested by Ellis, Giele, Kunszt, Melnikov and Zanderighi [69, 76] and that of Ita and Ozeren [77]. The principle is rather simple:

1. First we generate all the Feynman diagrams  $D_i$  for a given  $n$ -parton amplitude, separating each one into a colour factor denoted by  $C_i$  and a kinematic factor containing the Lorentz structure denoted by  $K_i$ :

$$\mathcal{A}_n = \sum_{i=1}^{N_{\text{dia}}} D_i = \sum_{i=1}^{\hat{N}_{\text{dia}}} C_i K_i, \quad (2.8)$$

where  $N_{\text{dia}}$  is the total number of diagrams and  $\hat{N}_{\text{dia}}$  is the number of diagrams excluding ones with four point interactions<sup>1</sup>. Each diagram's colour factor  $C_i$  is a known linear combination of trace factors  $T_c(\{a\})$  with coefficients  $F_{ci}$ :

$$C_i = \sum_c T_c(\{a\}) F_{ci}. \quad (2.9)$$

For clarity we omit the loop superscript on the colour dressed amplitude  $\mathcal{A}_n$  for the remainder of this section.

2. Secondly we write all possible primitive amplitudes  $P_i$  as combinations of colour-stripped diagrams:

$$P_i = \sum_{j=1}^{\hat{N}_{\text{dia}}} M_{ij} K_j, \quad i \in \{1, 2, \dots, N_{\text{pri}}\}, \quad N_{\text{pri}} = N_{\text{pri}}^{[m]} + N_{\text{pri}}^{[f]} \quad (2.10)$$

$$N_{\text{pri}}^{[f]} = (n-1)!, \quad N_{\text{pri}}^{[m]} = \begin{cases} (n-1)!, & n_q = 0 \\ \frac{1}{2} n_q (n-1)!, & n_q = 2, 4, \dots \end{cases} \quad (2.11)$$

where  $n_q$  is the number of external quarks. Obviously the set  $\{P_i\}$  is overcomplete and  $N_{\text{pri}}$  is only an upper bound for the number of primitives. The coefficients  $M_{ij}$  have entries of  $\pm 1$  and 0 depending on how the parent diagram representing the ordered primitive amplitude  $P_i$  matches onto the kinematic topology of  $K_j$  (1 – even-ordered,  $-1$  – odd-ordered, 0 – no match). Figure 2 depicts an example of the matching for the primitive amplitude  $A_5^{[m]}(1_{\bar{d}}, 2_u, 3_{\bar{u}}, 4_g, 5_d)$ , the notion of odd and even is taken with respect to the colour ordered Feynman rules (see for instance Ref. [78]).

If some diagrams are known to have additional non-trivial relations, this information can be included at this step to reduce the number of columns in  $M_{ij}$ . For instance Furry's theorem can be used on fermionic loops to obtain additional simplifications.

---

<sup>1</sup>The kinematic parts  $K_i$  are understood to contain contributions from both 3-gluon and 4-gluon vertices.

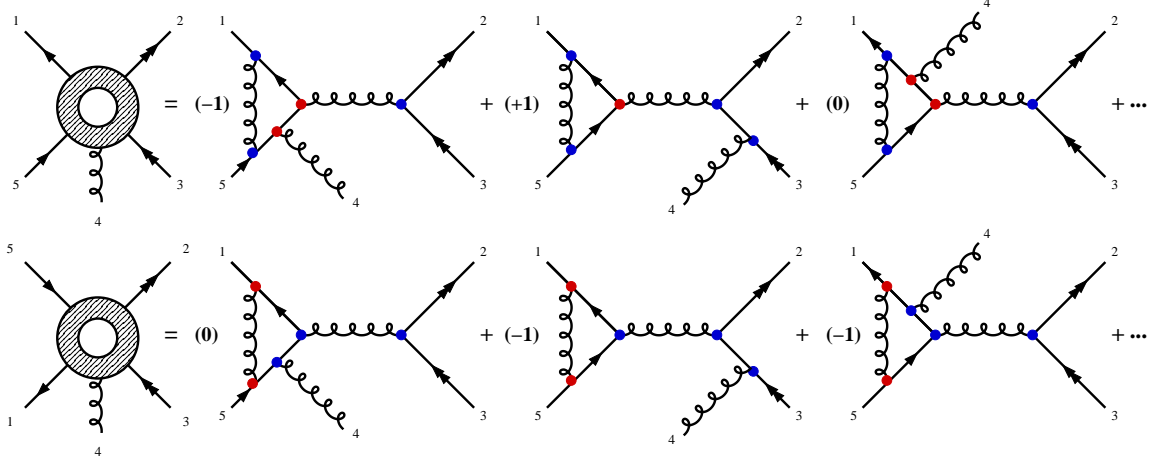


**Figure 2.** Matching Feynman diagrams to the primitive amplitudes  $A_5^{[m]}(1_{\overline{d}}, 2_u, 3_{\overline{u}}, 4_g, 5_d)$  and  $A_5^{[m]}(1_{\overline{d}}, 4_g, 3_{\overline{u}}, 2_u, 5_d)$ . Each vertex is either ordered (red) or unordered (blue) with respect to the primitive in question. A diagram contributes with a coefficient  $-1$  when it contains an odd number of unordered vertices and  $+1$  otherwise. Any diagram which cannot be obtained from the original primitive by “pinching” and “pulling” operations will have a 0 coefficient.

3. The rank of the matrix obtained at the previous step defines the number of independent primitive amplitudes, which is usually much smaller than the initial upper bound.

$$\hat{N}_{\text{pri}} = \text{rank } M, \quad \hat{N}_{\text{pri}} \leq N_{\text{pri}}, \quad \hat{N}_{\text{pri}} \leq \hat{N}_{\text{dia}} \quad (2.12)$$

To solve the equation (2.10) it is convenient to consider the augmented matrix  $\hat{M} = [M | -\mathbb{1}]$ , where  $\mathbb{1}$  is the  $N_{\text{pri}}$ -dimensional identity matrix. By putting it into reduced row echelon form (RREF), we get a solution of (2.10) as the upper  $\hat{N}_{\text{pri}}$  rows of  $\text{RREF}(\hat{M})$ . The lower  $N_{\text{pri}} - \hat{N}_{\text{pri}}$  rows will contain the left null space of the matrix  $M$ , which encodes relations between primitive amplitudes. A solution with a minimal basis of primitives is guaranteed by the properties of the RREF operation.

$$K_i = \sum_{j=1}^{\hat{N}_{\text{pri}}} B_{ij} \hat{P}_j, \quad \{\hat{P}_j\}_{\hat{N}_{\text{pri}}} \subset \{P_j\}_{N_{\text{pri}}}. \quad (2.13)$$

4. After substituting solution (2.13) into (2.8) and expressing the colour factors  $C_i$  using the trace basis  $T_c$  we can form the partial colour amplitudes in terms of independent primitive amplitudes  $\hat{P}_i$  as in (2.3),

$$\mathcal{A}_n = \sum_c T_c(\{a\}) A_{n;c} = \sum_c T_c(\{a\}) \sum_{j=1}^{\hat{N}_{\text{pri}}} Q_{cj} \hat{P}_j, \quad Q_{cj} = \sum_{i=1}^{\hat{N}_{\text{dia}}} F_{ci} B_{ij}. \quad (2.14)$$

We are now free to use the result of the primitive decomposition, eq. (2.14), to evaluate the colour sums in eqs. (2.6) and (2.7) in terms of primitive amplitudes.

Though this procedure involves generation of Feynman diagrams, only topologies of graphs are required making the application even to a relatively high multiplicity straightforward. Nevertheless the generic algorithm outlined above can be further improved. The four gluon vertex carries no additional information as far as colour is concerned and can be ignored leading to a substantial speed up. In general, since we are only looking for one specific solution of (2.10), any subset of diagrams which results in the matrix with the same rank as  $M_{ij}$  will be sufficient to obtain the correct form of (2.14).

The number of independent primitive amplitudes for the pure gluon and single fermion pair channels follows the well known structure outlined in references [3, 68]. Our approach to the fermion loops exploiting Furry type symmetries differs from that of Ita and Ozeren [77] explaining the smaller number of primitive amplitudes we obtain in the multi-fermion channels. Table 1 lists the number of primitives for all channels required for  $\leq 5$  jet production. As an example we show the fermion loop contribution to the six-quark amplitude

$$A_{6q}(1_{\bar{u}}, 2_u, 3_{\bar{d}}, 4_d, 5_{\bar{s}}, 6_s) = A_{6q}^{\text{mixed}} + n_f A_{6q}^{q\text{-loop}}$$

expressed in terms of 4 primitive amplitudes:

$$A_{6q}^{q\text{-loop}} = \frac{1}{N_c} \left( T_3 + T_4 - T_1 N_c - \frac{1}{N_c} T_6 \right) \times A^{[f]}(123456) + \frac{1}{N_c} (T_5 - T_3) \times A^{[f]}(124365) \\ + \frac{1}{N_c} \left( 2T_5 - T_2 N_c - \frac{1}{N_c} T_6 \right) \times A^{[f]}(125634) + \frac{1}{N_c} (T_5 - T_4) \times A^{[f]}(126534)$$

where  $T_i$  are the basis of colour factors

$$\begin{aligned} T_1 &= \delta_{16} \delta_{32} \delta_{54}, & T_2 &= \delta_{14} \delta_{36} \delta_{52}, & T_3 &= \delta_{12} \delta_{36} \delta_{54}, \\ T_4 &= \delta_{14} \delta_{32} \delta_{56}, & T_5 &= \delta_{16} \delta_{34} \delta_{52}, & T_6 &= \delta_{12} \delta_{34} \delta_{56}. \end{aligned}$$

	$A^{[0]}$	$A^{[m]}$	$A^{[f]}$		$A^{[0]}$	$A^{[m]}$	$A^{[f]}$
$\mathcal{A}_4(g, g, g, g)$	2	3	3	$\mathcal{A}_5(g, g, g, g, g)$	6	12	12
$\mathcal{A}_4(\bar{d}, d, g, g)$	2	6	1	$\mathcal{A}_5(\bar{d}, d, g, g, g)$	6	24	6
$\mathcal{A}_4(\bar{d}, d, \bar{u}, u)$	1	4	1	$\mathcal{A}_5(\bar{d}, d, \bar{u}, u, g)$	3	16	3
	$A^{[0]}$	$A^{[m]}$	$A^{[f]}$		$A^{[0]}$	$A^{[m]}$	$A^{[f]}$
$\mathcal{A}_6(g, g, g, g, g, g)$	24	60	60	$\mathcal{A}_7(g, g, g, g, g, g, g)$	120	360	360
$\mathcal{A}_6(\bar{d}, d, g, g, g, g)$	24	120	33	$\mathcal{A}_7(\bar{d}, d, g, g, g, g, g)$	120	720	230
$\mathcal{A}_6(\bar{d}, d, \bar{u}, u, g, g)$	12	80	13	$\mathcal{A}_7(\bar{d}, d, \bar{u}, u, g, g, g)$	60	480	75
$\mathcal{A}_6(\bar{d}, d, \bar{u}, u, \bar{s}, s)$	4	32	4	$\mathcal{A}_7(\bar{d}, d, \bar{u}, u, \bar{s}, s, g)$	20	192	20

**Table 1.** The number of contributing independent primitive amplitudes at tree-level ( $A^{[0]}$ ) and at one-loop for the mixed ( $A^{[m]}$ ) and fermion loop ( $A^{[f]}$ ) cases. Like flavour amplitudes for multiple fermions are obtained by symmetrization and therefore contain larger bases of primitives.

In cases where the final state has a Bose symmetry (i.e. for gluons in the final state) the colour summation can be further simplified. Since the phase space integration is symmetric under



permutations of the outgoing gluons, it is possible to work with a ‘de-symmetrized’ version of the squared matrix elements and achieve the symmetrization through the phase space integration [79],

$$\begin{aligned}\sigma_{gg \rightarrow n(g)}^V &= \int d\text{LIPS}_n \sum_{c=1}^{(n-2)!} \sum_{c'=1}^{(n-1)!/2} A_{n;c}^{(0)\dagger} \cdot C_{cc'}^{(1)} \cdot A_{n;c'}^{(1)} \\ &= \frac{(n-2)!}{2} \int d\text{LIPS}_n \sum_{c=1}^{(n-2)!} \sum_{c'=1}^{n-1} A_{n;c}^{(0)\dagger} \cdot C_{cc'}^{(1),\text{dsym}} \cdot A_{n;c'}^{(1),\text{dsym}}\end{aligned}\quad (2.15)$$

where  $d\text{LIPS}_n$  denotes the Lorentz invariant phase space measure of the  $n$  parton final state. In the case of the gluonic channels the saving is significant and brings the number of independent primitive amplitudes from  $\frac{1}{2}(n-1)!$  down to  $(n-1)$ . The de-symmetrized colour matrices  $C^{(1),\text{dsym}}$  have been computed and implemented in NJET for all gluonic channels, the fermionic channels however do not improve to the same extent and are implemented in the standard fashion.

We note that the number of independent primitives is significantly reduced in the case of the leading colour approximation where additional symmetries can be exploited. A complete investigation of the validity of such an approximation remains for a future study.

### 2.3 Cache system for tree amplitudes

The various primitives contributing to a full-colour helicity summed squared matrix element differ with respect to the external helicities, the permutations of the external legs and the loop content. On the other hand, every primitive is constructed by sewing together partial tree-level amplitudes. Therefore partial trees that agree in momenta, flavour and helicities of both external legs and internal legs can be reused for different primitive amplitudes.

An example is illustrated in Figure 3 for a triangle cut of a six-point amplitude with one external quark line and mixed loop content. Flipping the helicity of the fourth external gluon and permuting the fifth and sixth external leg leaves the five point partial tree amplitudes  $A(\ell_{1;g}^\pm, 1_q^-, 2_g^+, 3_g^-, \ell_{4;\bar{q}}^\pm)$  unchanged.

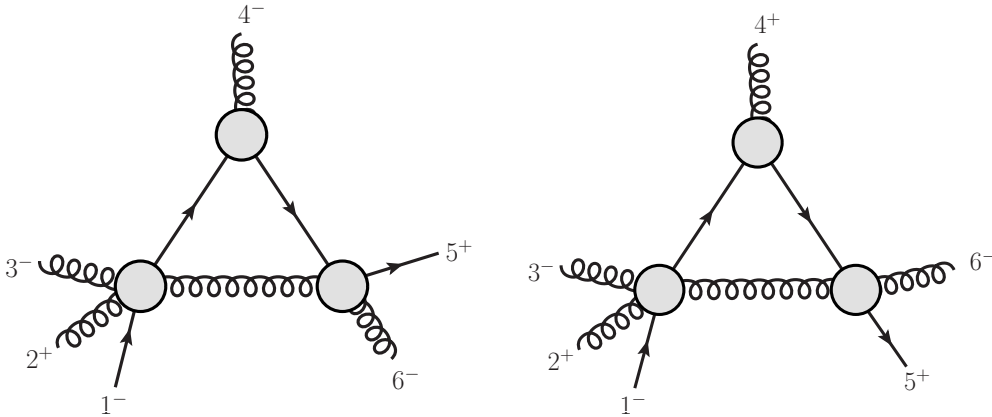


**Figure 3.** Triple cut for two primitives with different helicity and ordering of external legs. The partial trees  $A(\ell_{1;g}^\pm, 1_q^-, 2_g^+, 3_g^-, \ell_{4;\bar{q}}^\pm)$  are the same for both primitives.

The relation between external permutation and loop momentum requires some comments. Let  $\tau \in \{2, 3, 4, 5\}$  denote the topology of the cut, say bubbles, triangles, boxes and pentagons, and  $\mathcal{K}_\tau = \{k_1, \dots, k_{\tau-1}\}$  a set of  $\tau - 1$  external momentum sums which determine the kinematic invariants of the cut. Since the on-shell loop momentum for a distinct topology depends on  $\tau$  and on the full set  $\mathcal{K}_\tau$ . A necessary condition to reuse loop momenta, is to find equal sets of external momentum sums  $\mathcal{K}_\tau$ . In the above example,  $\mathcal{K}_\tau$  is the same for both permutations  $\{\{1, 2, 3\}, \{4\}, \{5, 6\}\} = \{\{1, 2, 3\}, \{4\}, \{6, 5\}\}$ . Analogously all six permutations of the first three legs would again lead to the same loop momenta. While the agreement of the external momenta and the flavour and helicity structure of all legs is required directly by the partial tree amplitude itself, the loop momentum matching depends on the topology and the permutation of all external legs. Hence, the knowledge of the cuts, permutations, flavours and helicities allows us to assign every partial tree amplitude a unique number which we use in a binary tree to cache those trees efficiently.

Since one has to sum over the helicities of the partons circulating in the loop to determine a specific cut, we store always a block of four amplitudes belonging to the four helicity combinations  $(+, +)$ ,  $(+, -)$ ,  $(-, +)$  and  $(-, -)$  of the two partons connecting the amplitude to the loop.

## 2.4 Universal Pole Structure and Scheme Dependence

All basic quantities in NGLUON are computed in the four-dimensional helicity (FDH) scheme. For consistency checks and the conversion to the conventional dimensional regularisation (CDR) scheme the universal structure of infrared (IR) and ultraviolet (UV) poles is required. The universal pole structure is known and can be derived from Refs. [80, 81]. For the colour summed squared amplitudes in massless QCD the result in the FDH scheme reads:

$$\begin{aligned} \text{Re}(\mathcal{A}^{(0)\dagger} \cdot \mathcal{A}_U^{(1),FDH}) &= \frac{1}{\epsilon^2} \left( N_c n_g + \frac{N_c^2 - 1}{2N_c} n_q \right) g_s^2 |\mathcal{A}^{(0)}|^2 \\ &+ \sum_{i=1}^{n-1} \sum_{j=i+1}^n \frac{1}{\epsilon} \log \left( \frac{\mu_R^2}{-s_{ij}} \right) g_s^2 |\mathcal{A}_{ij}^{(0)}|^2 - \frac{1}{\epsilon} \left( \beta_0 + n_q \left( \frac{\beta_0}{2} - \frac{2}{3} \frac{N_c^2 - 1}{2N_c} \right) \right) g_s^2 |\mathcal{A}^{(0)}|^2 \\ &+ \text{finite terms}, \end{aligned} \quad (2.16)$$

where  $\mathcal{A}_U^{(1),FDH}$  denotes the unrenormalized one-loop amplitude in the FDH scheme,  $n_q$  is the number of external quarks and  $n_g$  is the number of external gluons and  $g_s$  is the QCD coupling constant. The first coefficient of the QCD beta function is given by  $\beta_0 = \frac{11N_c - 2N_f}{3}$ . The quantity  $|\mathcal{A}_{ij}^{(0)}|^2$  is the colour correlated Born amplitude squared defined by

$$|\mathcal{A}_{ij}^{(0)}|^2 = \langle \mathcal{A}^{(0)\dagger} | T_i T_j | \mathcal{A}^{(0)} \rangle \quad (2.17)$$

where  $T_g = f^{abc}$  and  $T_q = T_{ij}^a$  and we followed the notation used in Ref. [80] to denote by  $|\mathcal{A}^{(0)}\rangle$  the leading order amplitude which can be understood as a vector in colour space. In order to provide results in the conventional dimensional regularisation (CDR) scheme we apply the conversion as determined by the universal IR and UV pole structure [80, 81]. The scheme conversion to CDR and the renormalization are both proportional to the Born amplitude. For convenience we list the

explicit relations between different prescriptions:

$$\frac{\text{Re} \left( \mathcal{A}^{(0)\dagger} \cdot (\mathcal{A}_R^{(1),FDH} - \mathcal{A}_U^{(1),FDH}) \right)}{g_s^2 |\mathcal{A}^{(0)}|^2} = -\frac{(n_g + n_q - 2)}{2} \left( \frac{\beta_0}{\varepsilon} - \frac{N_c}{3} \right) \quad (2.18)$$

$$\frac{\text{Re} \left( \mathcal{A}^{(0)\dagger} \cdot (\mathcal{A}_U^{(1),CDR} - \mathcal{A}_U^{(1),FDH}) \right)}{g_s^2 |\mathcal{A}^{(0)}|^2} = \frac{(n_g + n_q - 2)}{2} \frac{N_c}{3} - \frac{n_g N_c}{6} - \frac{n_q}{4N_c} (N_c^2 - 1) \quad (2.19)$$

$$\frac{\text{Re} \left( \mathcal{A}^{(0)\dagger} \cdot (\mathcal{A}_R^{(1),CDR} - \mathcal{A}_U^{(1),FDH}) \right)}{g_s^2 |\mathcal{A}^{(0)}|^2} = -\frac{(n_g + n_q - 2)}{2} \left( \frac{\beta_0}{\varepsilon} - \frac{N_c}{3} \right) - \frac{n_g N_c}{6} - \frac{n_q}{4N_c} (N_c^2 - 1) \quad (2.20)$$

where the subscript  $R$  denotes renormalized amplitudes.

### 3 Installation and Usage

The code can be obtained from <https://bitbucket.org/njet/njet/> as a tar archive. Alternatively the source can be obtained from the public git repository using

```
git clone https://bitbucket.org/njet/njet.git
```

Compilation for a wide variety of architectures and compilers is supported via a configure script generated with autoconf. The default set-up will be configured by simply using

```
./configure
```

which will scan your system for the required pre-requisites. Installation into a local directory structure is supported through the option `--prefix=<dir>`. Further useful options supported by the configure script are:

- `--enable-demo` Will compile some additional example programs which can be run with `make check` after the library has been successfully compiled. These demo programs illustrate the usage of the program and the correctness of the implementation. A sample output is given in appendix A.
- `--enable-5jet` Includes in the library the one-loop corrections for five jet production. Since the compilation requires a significant amount of memory the one-loop corrections for five jet production are disabled by default. It is not recommended to use this option with less than 4 GB of RAM.
- `--disable-cache` Per default the cache system is enabled. It allows caching of partial tree amplitudes to optimise the colour and helicity sums as described in section 2.3. Due to the way the cache is implemented an architecture dependent restriction is imposed on the total number of external particles. This is 6 on a 32-bit system and 13 on a 64-bit system. By using `--disable-cache` the cache can be disabled and the restrictions can be lifted however at the cost of losing some speed.

A complete list of possible options can be obtained using `--help`. Further details can be found in the `INSTALL` file in the root directory of the distribution. Once the configure script has successfully generated the makefiles compilation and installation can be performed with:

```
make
make install
```

Additionally,

```
make check
```

will run some basic tests to verify a correct installation. NJET is distributed with a version of QCDLoop for the evaluation of the scalar one-loop integrals and `qd` [82] to extend the precision of the floating-point arithmetic to quadruple precision.

### 3.1 Interface via the Binoth Les Houches Accord

Though the library can be interfaced directly, the simplest way to use it is to link via the Binoth Les Houches Accord (BLHA) interface [62]. Once correctly installed, a python script `njet.py` will interpret a user supplied “order file” to produce a “contract file” allowing the various processes and options to be passed to NJET. Several sample programs demonstrating the usage of this interface are included in the distribution with corresponding order files in the sub-directory `examples`. These examples can be compiled independently using the provided sample Makefile. In the following we briefly illustrate an example. The order file used in connection with the BLHA interface consists of two parts. The first part contains general settings such as matrix element type and regularisation scheme. The second part is a list of elementary sub-processes specified using PDG particle codes [83]. An example file for  $u\bar{u} \rightarrow 3\text{-jets}$  is shown below:

```
# order file for u ubar -> jets
MatrixElementSquareType CHsummed
CorrectionType          QCD
IRregularisation        CDR
AlphasPower             3
# process list
1 -1 -> 21 1 -1
1 -1 -> 21 2 -2
1 -1 -> 21 21 21
```

Assuming the order file is saved with the file name `OLE_order.lh` the command

```
njet.py -o OLE_contract.lh OLE_order.lh
```

will process it and creates a contract file `OLE_contract.lh`. The user should always check the generated contract file to ensure that all requested parameters and sub-processes have been recognized by NJET which is indicated in the generated contract file. Having a valid contract file one can use it with the standard BLHA interface functions which are declared in the `njet.h` header:

```

void OLP_Start(const char* filename, int* status);
void OLP_EvalSubProcess(int mcn, double* pp, double mur,
                        double* alphas, double* rval);

```

The conventions of their usage are described in [62], we outline here only the main features. Firstly the interface has to be initialized by calling the function `OLP_Start`, passing the file name of a contract file as a parameter. After the call, the second parameter `status` will contain 1 indicating the success or 0 indicating the failure of the initialization. In case of a successful initialization one can begin using `OLP_EvalSubProcess` to evaluate the subprocess `mcn` for a given phase space point with momenta `pp`, renormalization scale `mur` and strong coupling `alphas`. The integer `mcn` is the number of the process in the contract file (starting from 1). The momenta are passed through the one dimensional array `pp`. Note that in addition to the momentum for each parton also its mass is transferred, e.g.

$$pp[5n] = \{p_0^0, p_0^1, p_0^2, p_0^3, m_0, p_1^0, p_1^1, p_1^2, p_1^3, m_1, \dots, p_{n-1}^0, p_{n-1}^1, p_{n-1}^2, p_{n-1}^3, m_{n-1}\}, \quad (3.1)$$

where  $p_n^i$  denotes the  $i$ -th momentum component of the  $n$ -th parton. The result is returned through the array `rval` with the following order of elements:  $1/\epsilon^2$ -pole,  $1/\epsilon$ -pole, finite part, tree amplitude. If requested in the order file, the `rval` array will contain three additional elements: relative accuracy of the  $1/\epsilon^2$ -pole, relative accuracy of the  $1/\epsilon$ -pole, and relative accuracy of the finite part.

### 3.1.1 Additional BLHA options

In addition to the standard options (see Ref. [62]) `njet.py` allows the following additional options to control the interface.

- `NJetType` [default = loop]  
`loop`, `loops` or `tree` may be specified to determine the type of the squared matrix element returned. `loop` and `tree` are conventional colour summed squared amplitudes for one-loop and tree contributions respectively. `loops` returns the de-symmetrized sums if available otherwise the standard one-loop sum is returned. A more advanced usage is to specify a list separated by a '-' of a process number followed by a '.' and the type required for that process (see example in supplied demo program `examples/DSYMtest`).
- `NJetReturnAccuracy` [default = no]  
 If set to `yes`, the scaling test is used to estimate the accuracy and the result is returned in the output array making it three entries longer.
- `NJetSwitchAcc` [default = 1e-5]  
 Used to set the relative accuracy at which higher precision floating point arithmetics will be used to evaluate the phase space point if double precision has not produced the desired accuracy. To account for the statistical nature of the scaling test it is recommended to specify 1 or 2 digits more than the required accuracy.
- `NJetNf` [default = 5]  
 Set the number of light quark flavours circulating in the fermion loops.

A full documentation of the usage of `njet.py` can be found in `lh/LH.txt`.

### 3.2 The NParton library for multi-parton primitives

Also provided with the package is the NParton class for the evaluation of arbitrary multi-parton primitive amplitudes both at tree-level and at one loop. The usage is demonstrated in an example code compiled into the `src-nparton` directory: `NParton-test.cpp`.

#### 3.2.1 Initialization and Namespaces

NParton is designed such that both double and quadruple precision can be used in parallel in the same program. In order to achieve this, different namespaces `NJet_sd` and `NJet_dd` are used for single double and double double (=quadruple) respectively. Inclusion of the header file `src-nparton/NParton-multiprec.h` will take care of the necessary declarations.

Both classes require loop integrals and other parameters to be initialized before they can be used which is done by creating the static objects

```
static NJet_sd::Initialize global_init_sd;  
static NJet_dd::Initialize global_init_dd;
```

before the start of the main program.

#### 3.2.2 Constructor

The calculation of the primitive amplitudes is hidden in the class NParton. The class constructor only requires one integer argument specifying the number of external legs. The namespace for the required accuracy must also be specified, e.g.

```
NJet_sd::NParton primitive(int npartons);
```

for double precision and,

```
NJet_dd::NParton primitive(int npartons);
```

for quadruple precision.

#### 3.2.3 Member functions

The actual calculation is controlled through member functions of the NParton class. The relevant functions are:

- `void setAmp(double moms[][4], int[] flavs)`

This function sets the momenta and flavour of the external legs being the same for all helicity configurations of one primitive amplitude. The four-momenta are entered as an array of four-vectors with the energy in the zeroth component according to  $(E, p_x, p_y, p_z)$ . The list of flavours is specified as follows: 0 for a gluon,  $(-i)$  for each (anti-)quark with  $i \in \{1, 2, \dots, N_{q\bar{q}}\}$  and  $N_{q\bar{q}}$  the total number of external quark lines. Due to fermion and flavour number conservation the quarks must always appear as quark–anti-quark pairs. Each quark line must be labelled with a different integer. The primitive amplitudes calculated thus correspond to the case that all quark flavours are different. The equal flavour case can be obtained from these results through an appropriate anti-symmetrization. Since QCD conserves

the flavour number the fermion lines are not allowed to cross in the primitive amplitudes. A valid choice would be, for example,  $\{1, 0, 2, -2, -1\}$  while  $\{1, 0, 2, -1, -2\}$  would however give an error.

- `void eval(int[] hels, int ptype)`

`void eval(int hels, int ptype)`

After a previous call of `setAmp` this function evaluates a single primitive amplitude. The first argument is a list of helicities specified by  $\pm 1$  for each parton. Alternatively the helicity can be given as a single integer between 0 and  $2^n - 1$  which is very convenient to loop over. The second argument selects either the mixed or the fermion loop primitive amplitude using the internally defined constants `NParton::mixed` and `NParton::qloop`.

- `std::complex<double> evalTree(int[] hels)`

`std::complex<double> evalTree(int hels)`

Similar to the `eval` function except that only the tree amplitude is evaluated. As `eval` this function requires a previous call of `setAmp`. The value of the tree-level helicity amplitude is returned.

- `std::complex<double> getAmp(int p)`

`std::complex<double> getAbsErr(int p)`

`std::complex<double> getRelErr(int p)`

After calling the `eval` function the various components of the amplitudes and their absolute and relative numerical uncertainty can be accessed with these functions. The different contributions are obtained by setting the variable `p` to one of the predefined constants:

<code>NParton::eps0</code>	returns the finite part,
<code>NParton::eps1</code>	returns the coefficient of the $1/\epsilon$ pole,
<code>NParton::eps2</code>	returns the coefficient of the $1/\epsilon^2$ pole,
<code>NParton::tree</code>	returns the tree-level amplitude,
<code>NParton::rational</code>	returns the rational part,
<code>NParton::cutconstructible</code>	returns the cut-constructible part.

- `void IRcheck()`

After calling the `eval` function this function will check the poles against known universal pole structure. The relative error of both  $1/\epsilon^2$  and  $1/\epsilon$  poles compared with the analytic formulae will be displayed.

- `void refine(double moms, dd_real moms_dd)`

This function converts a double precision phase-space point to quadruple precision to enable the calculation in quadruple precision using `NJet_dd::NParton`.

- `void setMuR2(double MuR2)`

Used to set the renormalization scale squared,  $\mu_R^2$ .

- `std::string ProcessStr()`

Returns a string with the current flavour and helicity structure. This gives the state of the last `evalAmp` call.



Process	Reference
$pp + 2j$ (all $2 \rightarrow 2$ with colour summation)	[84]
$5g$	[85]
$q\bar{q} + 3g$	[68]
$n(g)$ (finite)	[86]
$n(g)$ (MHV)	[87]
$q\bar{q} + n(g)$ (finite)	[88]

**Table 2.** Cross checks against analytic expressions known in the literature.

With the exception of the `refine` function, when using `NJet_dd::NParton`, `double` should be replaced with `dd_real`.

## 4 Results

### 4.1 Validation

To assess the correctness of our implementation we performed a series of highly non-trivial tests. The first test is to check the universal structure of the IR and UV poles (see section 2.4). Both at the level of primitive amplitudes and colour summed amplitudes we find for all the processes we have tested perfect agreement for the  $1/\epsilon^2$  and  $1/\epsilon$  poles where  $D = 4 - 2\epsilon$  with  $D$  denoting the dimension of space-time. As far as the UV poles are concerned this check tests a linear combination of the coefficients of the two-point scalar integrals. The correct IR structure is sensitive to the coefficients of all IR divergent scalar three- and four-point integrals. Since the coefficients of the scalar integrals are all calculated the same way reproducing the correct IR and UV structure provides a strong test on the entire cut-constructible part.<sup>2</sup> However the rational part of the amplitude cannot be tested in this way. To verify the non-trivial rational part a large number of cross checks against known processes at individual phase-space points has been performed. We have confirmed the results for primitive amplitudes for specific helicity configurations with the known analytic results listed in table 2. The checks of the primitive amplitudes in pure gauge theory with the all  $n$  multiplicity formulae in [86, 87] have already been presented in Ref. [1]. Primitive amplitudes with one external quark pair have been tested against the explicit formulae for  $q\bar{q} + 3g$  given in Ref. [68]. We find complete agreement for all independent primitive amplitudes and all independent helicity configurations for these five-point amplitudes. The IR finite amplitudes with a single quark pair,  $A_n^{[m/f]}(q_1^-, g_2^+, \dots, \bar{q}_i^+, \dots, g_n^+)$ , have been computed analytically in Ref. [88] to all multiplicity. Direct comparisons over all possible configurations of the quark pair have been performed and in all cases we find good numerical agreement. The program `NParton-qqchecks` in the directory `src-tools` performs the comparisons with the analytic formulae listed above. In addition—with the exception of the six-gluon channel—we have cross checked numerically the colour summed interferences for all processes contributing to three and four jet production with results generated with HELAC-1LOOP [90]. We were also able to confirm results for the fermion loops with those generated from GOSAM [16]. These numerical checks against existing codes can be accessed through the sample

<sup>2</sup>We note that a possible small deviation of the numerically computed poles from the predicted pole structure due to numerical rounding errors could give some indication of the numerical accuracy of the current evaluation.



	NJET	BLACKHAT
$gg \rightarrow gggg$		
born	$+4.9769357371794838 \times 10^8$	$+4.976935736 \times 10^8$
$1/\epsilon^2$	$-1.7999999999999108 \times 10^1$	$-1.800000000 \times 10^1$
$1/\epsilon$	$-6.5144862057710100 \times 10^1$	$-6.514486205 \times 10^1$
finite	$-3.2130366101334992 \times 10^1$	$-3.213036625 \times 10^1$
$d\bar{d} \rightarrow gggg$		
born	$+2.1622011190045194 \times 10^5$	$+2.162201118 \times 10^5$
$1/\epsilon^2$	$-1.4666666666663076 \times 10^1$	$-1.466666667 \times 10^1$
$1/\epsilon$	$-5.8264471151950865 \times 10^1$	$-5.826447114 \times 10^1$
finite	$-4.3957884552089730 \times 10^1$	$-4.395788455 \times 10^1$
$d\bar{d} \rightarrow u\bar{u}gg$		
born	$+1.3745823177248822 \times 10^4$	$+1.374582317 \times 10^4$
$1/\epsilon^2$	$-1.133333333333261 \times 10^1$	$-1.133333333 \times 10^1$
$1/\epsilon$	$-4.8019618061344993 \times 10^1$	$-4.801961805 \times 10^1$
finite	$-3.7348157184728159 \times 10^1$	$-3.734815718 \times 10^1$
$d\bar{d} \rightarrow u\bar{u}s\bar{s}$		
born	$+3.6761219414819656 \times 10^1$	$+3.676121941 \times 10^1$
$1/\epsilon^2$	$-8.0000000000001386$	$-8.000000000$
$1/\epsilon$	$-2.6337813992821804 \times 10^1$	$-2.633781399 \times 10^1$
finite	$-6.7242846898320696 \times 10^{-1}$	$-6.724284689 \times 10^{-1}$

**Table 3.** Numerical comparison between NJET and the  $2 \rightarrow 4$  amplitudes given in Ref. [89].

program NJet-demo. Sample output is provided in appendix A. In case of four jet production full agreement has also been found with results for a single phase-space point provided by BLACKHAT [89]. The explicit outcome is shown in Table 3. The results in Ref. [89] are given up to ten decimal digits. Apart from the gluonic channel we recover all digits using double precision. For the pure gluon channel the error estimate of the numerical evaluation obtained via the scaling test gives,

$$A_{6g}^{(1),\text{finite}} = -3.2130366101334992 \times 10^1 \pm 3 \times 10^{-8},$$

hence all reliable digits are in agreement with the BLACKHAT result. When evaluated in quadruple precision all digits are in agreement:

$$A_{6g}^{(1),\text{finite}} = -3.2130366250275191 \times 10^1 \pm 2 \times 10^{-13}.$$

The full set of quadruple precision checks can be reproduced using `NJet-demo-dd --BlackHat4j`.

It is important to note that the scalar one-loop integrals are evaluated in double precision which limits the final accuracy of NJET to 16 decimal digits even when quadruple precision is used.

Given the large number of checks passed by NJET we are confident the library produces reliable results for one-loop amplitudes in massless QCD.

Since the amplitudes for virtual corrections to five-jet production have not been presented in the literature before, we give the numerical values for the evaluation at a single phase space point in appendix B.

## 4.2 Accuracy

Given the complexity of the calculations performed in the NJET library it is important to have a precise understanding of the numerical accuracy. We have performed a number of tests on the output of both primitive amplitudes and colour summed squared matrix elements. By performing the scaling test as described in Ref. [1] we can reliably estimate the number of correct digits returned by the program.

Figure 4 shows for four channels contributing to four jet production the distribution of the estimated accuracy. In total  $10^4$  phase space points were generated. The accuracy is defined by

$$\text{Accuracy}(\mathcal{A}(p, \mu_R)) = \log_{10} \left( 2 \frac{\mathcal{A}(p, \mu_R) - x^{n-4} \mathcal{A}(xp, x\mu_R)}{\mathcal{A}(p, \mu_R) + x^{n-4} \mathcal{A}(xp, x\mu_R)} \right), \quad (4.1)$$

where  $p$  are the external momenta,  $\mu_R$  is the renormalization and  $x$  is the scaling parameter. This definition gives a direct measure of the valid digits. The phase space points were generated with a sequential splitting algorithm as described in [91]. For large multiplicities the algorithm prefers collinear configuration. Compared to a flat phase space generation we believe that this simulates better what will actually happen in a phase space integration. A weak phase space cut of  $|p_i \cdot p_j| > s \times 10^{-2}$  was made for a centre-of-mass energy of  $s = 7$  TeV. For the most complex channels around 1% of points must be re-evaluated in quadruple precision. Some of them are related to small Gram determinants but these are not the only sources of numerical instability within the algorithm. As we consider channels with more quarks, and therefore lower maximum tensor rank, the accuracy improves considerably. For these processes all evaluations pass the threshold accuracy of  $10^{-4}$  after quadruple precision has been used. Similar, though significantly improved behaviour, is observed for the lower multiplicity channels, plots of the distributions can be found in Ref. [67].

Figure 5 shows an identical analysis for two channels contributing to five jet production. For the seven gluon amplitude we observe an increasing number of instabilities such that the time to re-evaluate with quadruple precision becomes noticeable. Again increasing the number of fermion pairs improves the situation a lot. Performing the floating point arithmetics in quadruple precision 99.99% of points achieve the required 4 digits of accuracy. It might be required switching to octuple precision when performing phase-space integration of virtual amplitudes of this complexity.

## 4.3 Speed Tests

An advantage of the recursive construction of ordered tree-level amplitudes within NGLUON is that the computation of multi-fermion primitives scales polynomially with time. The scaling properties of the algorithm for up to three quark pairs with fixed parton ordering and up to 13 external legs, the maximally allowed number with the cache system turned on, are shown in Figure 6. For simplicity we restrict the analysis to amplitudes with neighbouring quark pairs,  $A_n(q_1, \bar{q}_1, \dots, q_k, \bar{q}_k, g_{2k+1}, \dots, g_n)$  for  $k$  quark lines. The times are averaged over all  $2^n$  helicity configurations including amplitudes that vanish trivially by helicity conservation along fermion lines. The scaling behaviour reflects that the cache system has been used to improve the efficiency of the helicity sum and varies between

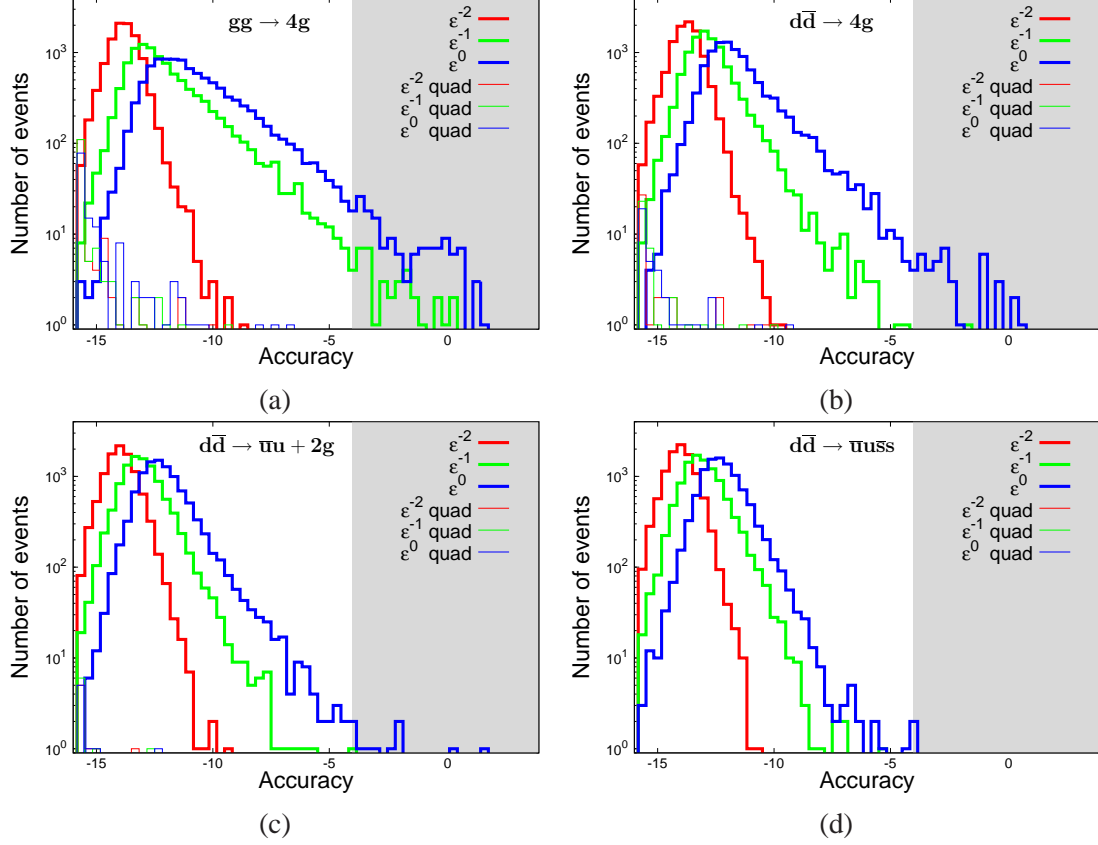


**Figure 4.** Accuracy for 4-jet amplitudes: (a) shows the six gluon process, (b) the  $d\bar{d} \rightarrow 4g$  process, (c)  $d\bar{d} \rightarrow \bar{u}u + 2g$  and (d) the six unlike quark pair process. The thicker histograms show computations in double precision whereas the thinner curves show the distribution in quadruple precision for points which did not pass the relative accuracy of  $10^{-4}$  when calculated in double precision (region marked by the shaded area). Red histograms show the  $\frac{1}{\epsilon^2}$  poles, green histograms the  $\frac{1}{\epsilon}$  and blue histograms the finite part of the amplitudes.

$n^{4.5}$  and  $n^{6.0}$ . In the asymptotic region the algorithm employed in NGLUON is known to scale as  $n^8$  for the mixed loop content [1]. For the closed quark loop this is reduced to  $n^7$  since the coupling of external off-shell currents to the fermion loop goes exclusively via three-point vertices. We find that the asymptotic scaling behaviour is reached at extremely high multiplicities ( $> 20$  legs) and has little practical relevance. The asymptotic scaling holds also for the average of configurations with non-neighbouring quark pairs. Of course, the timings of individual amplitudes are sensitive to a non-vanishing quark antiquark separation. One observes the expected pattern of a speed up in the closed quark loop case and a slow down in the mixed quark gluon loop. A more detailed analysis for non-neighbouring quark configurations is given in [66].

Table 4 shows the timing estimates for colour and helicity summed virtual corrections for all sub-processes of multi-jet production with up to 5 jets. The times are quoted for single double precision,  $T_{sd}$ , and including corrections using quadruple precision in order to achieve an overall accuracy of  $10^{-4}$ ,  $T_4$  digits. We also show the fraction of points which did not pass the relative

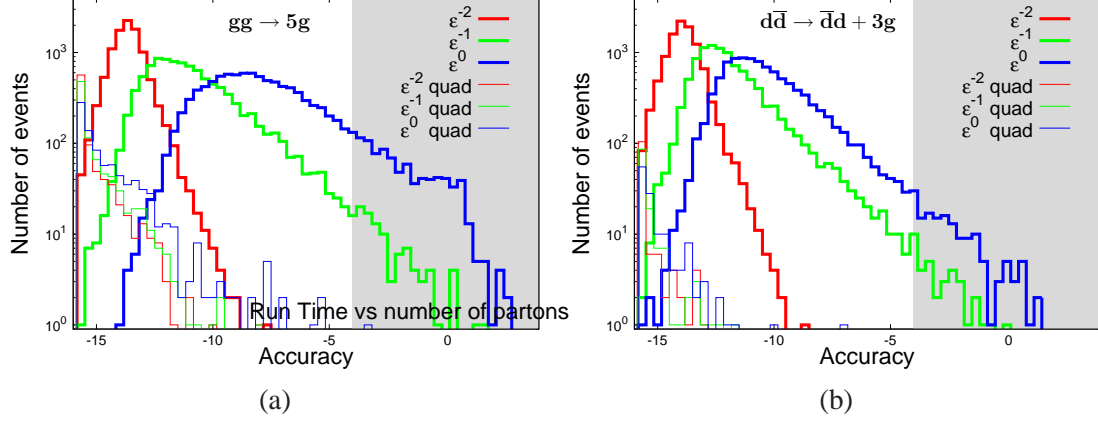


**Figure 5.** Accuracy for 5-jet amplitudes: (a) shows the seven gluon process and (b) the  $d\bar{d} \rightarrow \bar{d}d + 3g$  process. The thicker histograms show computations in double precision whereas the thinner curves show the distribution in quadruple precision for points which did not pass the relative accuracy of  $10^{-4}$  when calculated in double precision. Red histograms show the  $\frac{1}{\epsilon^2}$  poles, green histograms the  $\frac{1}{\epsilon}$  and blue histograms the finite part of the amplitudes.

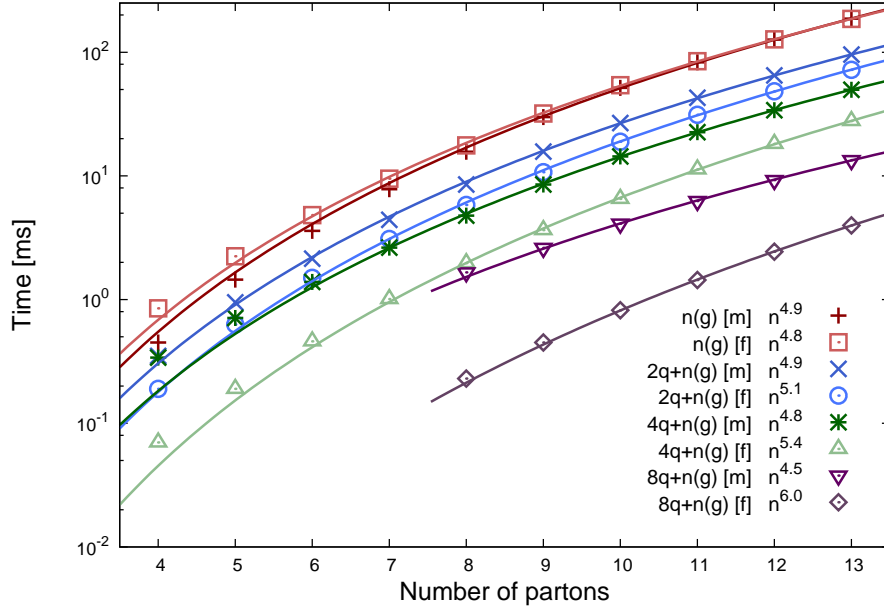


**Figure 6.** Estimated evaluation time for primitive amplitude with 0, 1, 2 and 4 fermion lines averaged over the total number of helicities as a function of the number of external legs. Both mixed quark gluon loop and closed quark loop are shown. The curves are a fit to the polynomial  $f(n) = an^b$ . The exponent  $b$  can be read off from the legend. The times were measured on an Intel(R) Core(TM)2 Duo CPU E8400 @ 3.00GHz.

accuracy when evaluated in double precision. All times include the two evaluations necessary to obtain the accuracy estimate via the scaling test. Times have been obtained using the clang v2.8 compiler. The time estimated for the reevaluation using quadruple precision is based on the

process	$T_{sd}[s]$	$T_{4 \text{ digits}}[s]$	(% fixed)	process	$T_{sd}[s]$	$T_{4 \text{ digits}}[s]$	(% fixed)
4g	0.030	0.030	(0.00)	5g	0.22	0.22	(0.22)
2u2g	0.032	0.032	(0.00)	2u3g	0.34	0.35	(0.06)
2u2d	0.011	0.011	(0.00)	2u2d1g	0.11	0.11	(0.00)
4u	0.022	0.022	(0.00)	4u1g	0.22	0.22	(0.03)

process	$T_{sd}[s]$	$T_{4 \text{ digits}}[s]$	(% fixed)	process	$T_{sd}[s]$	$T_{4 \text{ digits}}[s]$	(% fixed)
6g	6.19	6.81	(1.37)	7g	171.3	276.7	(8.63)
2u4g	7.19	7.40	(0.38)	2u5g	195.1	241.2	(3.25)
2u2d2g	2.05	2.06	(0.08)	2u2d3g	45.7	48.8	(0.88)
4u2g	4.08	4.15	(0.21)	4u3g	92.5	101.5	(1.29)
2u2d2s	0.38	0.38	(0.00)	2u2d2s1g	7.9	8.1	(0.23)
2u4d	0.74	0.74	(0.00)	2u4d1g	15.8	16.2	(0.29)
6u	2.16	2.17	(0.02)	6u1g	47.1	48.6	(0.41)

**Table 4.** Timing estimates in seconds for full colour and helicity summed virtual corrections.  $T_{sd}$  is the time for evaluation in double precision,  $T_{4 \text{ digits}}$  is the average time estimated to obtain a result correct to 4 digits using the phase space cuts of section 4.2. All times include the two evaluations necessary to obtain the accuracy estimate via the scaling test and were obtained on an Intel(R) Xeon(R) CPU E3-1240 @ 3.30GHz.

	$gg \rightarrow 2g$	$gg \rightarrow 3g$	$gg \rightarrow 4g$	$gg \rightarrow 5g$
standard sum	0.03	0.22	6.19	171.31
de-symmetrized	0.03	0.07	0.57	3.07

**Table 5.** Timing estimates in seconds for the de-symmetrized colour and helicity summed gluonic channels. All times include the two evaluations necessary to obtain the accuracy estimate via the scaling test and were obtained on an Intel(R) Xeon(R) CPU E3-1240 @ 3.30GHz.

percentage of rescued points from the accuracy tests in the previous section. On average quadruple precision evaluation was found to be between 7 and 8 times longer than double precision. We stress that even in the worst case of the seven gluon amplitude the required reevaluation only doubles the total run time.

Table 5 shows the evaluation times using the de-symmetrized colour sums for the pure gluonic channels which exploit the Bose symmetry of the final state. Though these channels benefit the most from this treatment the complex channels with a single fermion pair would also see a considerable speed up. Again we stress that these de-symmetrized sums contain the same full colour information as the standard ones after the integration over the phase-space or equivalently after explicitly summing the  $\frac{1}{2}(n-2)!$  permutations of the final state gluons.

## 5 Conclusions

In this paper we have presented the C++ library NJET for the numerical evaluation of one-loop amplitudes for multi-jet production at hadron colliders. Using generalized unitarity together with off-shell recursion relations we were able to construct multi-fermion primitive amplitudes at a computational cost growing polynomially with time. Accuracy estimates obtained by applying a

momentum re-scaling test are used to ascertain when higher precision numerics are required to achieve a preset number of correct digits. A simple cache system allows the efficient computation of helicity and permutation sums.

In order to use the multi-fermion primitive amplitudes for NLO QCD computations the colour space information must be included. By matching primitive and partial amplitudes via Feynman diagrams we obtained full colour formulae for all channels contributing to  $\leq 5$  jet production. We employed Furry type symmetries and linear algebra techniques to minimize the number of primitive amplitudes appearing in the colour sums. Furthermore we made use of Bose symmetries in the final state to simplify the most complex all-gluon processes. Since the on-shell algorithm is particularly well suited to the computation of multi-gluon states which contain degenerate degrees of freedom we find a favourable performance in comparison to existing public one-loop amplitude generators.

The interface to the library is either directly to the primitive amplitudes using the `NParton` class or via a Binoth Les Houches Accord [62] to the colour and helicity summed amplitudes. The latter allows the library to be linked with existing parton level Monte Carlo programs which can combine the virtual and real radiation contributions to obtain full NLO predictions. The package presented here has been recently used to calculate three- and four jet cross sections at next-to-leading order in QCD [2]. This application nicely illustrates that the tool presented can be used for state of the art calculations. We also provide in Table 6 in the appendix benchmark points for all one-loop corrections required for the evaluation of the five jet cross section at next-to-leading order accuracy.

Future developments to include heavy quark corrections would be interesting.

The library NJET is publicly available from the project home page at <https://bitbucket.org/njet/njet>.

## Acknowledgments

We are grateful to Nigel Glover, Steven Wells, Rikkert Frederix and Marco Zaro for testing preliminary versions of the code. This work is supported by the Helmholtz Gemeinschaft under contract HA-101 (Alliance Physics at the Terascale) and by the European Commission through contract PITN-GA-2010-264564 (LHCPhenoNet).

## A Numerical cross checks

With `--enable-demo` used to configure the package two example programs are compiled into their respective source directories:

```
src-tools/NJet-demo
src-nparton/NParton-demo
```

`NParton-demo` is a short program showing how to use the `NParton` library by evaluating some one-loop multi-parton primitive amplitudes. The code found in `src-nparton/NParton-demo.cpp` has some comments to explain the functions calls.

A number of hard coded cross checks for the colour summed amplitudes can be found in the program `NJet-demo`. The individual checks can be accessed with command line options, simply type `NJet-demo --help` to see the available options.

For convenience we list the program output for the comparison with HELAC-1LOOP.

NJet-demo --Helac1l gives a numerical cross check with HELAC-1LOOP [90] for the available channels of dijet, three-jet and four-jet production. We find again good numerical agreement. The exact phase-space points for these checks are displayed to double precision when running the program. The results of these checks are as follows:

==== 0 --> g g g g ====

	NJet:	Helac1loop:	rel.diff.
born:	+1.4064482826874553e+02,	+1.4064482826874587e+02,	+2.4e-15
1/eps^2:	-2.7963100376599282e+01,	-2.7963100376599272e+01,	+3.8e-16
1/eps:	-2.4893580169045921e+00,	-2.4893580169051024e+00,	+2.0e-13
finite:	+2.2538771232905535e+01,	+2.2538771232905539e+01,	+1.6e-16

==== 0 --> u~ u g g ====

	NJet:	Helac1loop:	rel.diff.
born:	+3.8973755683505198e+00,	+3.8973755683505242e+00,	+1.1e-15
1/eps^2:	-5.5963473237272909e-01,	-5.5963473237273020e-01,	+2.0e-15
1/eps:	-2.2701782897620162e-01,	-2.2701782897620176e-01,	+6.1e-16
finite:	+1.5812149573186310e-01,	+1.5812149573186496e-01,	+1.2e-14

==== 0 --> u~ u d~ d ====

	NJet:	Helac1loop:	rel.diff.
born:	+5.5757038821628091e-01,	+5.5757038821628113e-01,	+4.0e-16
1/eps^2:	-4.9269566071365262e-02,	-4.9269566071365241e-02,	+4.2e-16
1/eps:	-4.9621618996857207e-02,	-4.9621618996857221e-02,	+2.8e-16
finite:	-2.8732424653763196e-02,	-2.8732424653763248e-02,	+1.8e-15

==== 0 --> u~ u u~ u ====

	NJet:	Helac1loop:	rel.diff.
born:	+5.4442906439318520e+01,	+5.4442906439318527e+01,	+1.3e-16
1/eps^2:	-4.8108336321631899e+00,	-4.8108336321631695e+00,	+4.2e-15
1/eps:	+3.8870984690869954e+00,	+3.8870984690871220e+00,	+3.3e-14
finite:	+2.3627403557985861e+01,	+2.3627403557985797e+01,	+2.7e-15

----- 2 --> 3 -----

==== 0 --> g g g g g ====

	NJet:	Helac1loop:	rel.diff.
born:	+5.0536873228500680e-02,	+5.0536873228500589e-02,	+1.8e-15
1/eps^2:	-1.2559719367246716e-02,	-1.2559719367246622e-02,	+7.5e-15
1/eps:	-6.5137043664892195e-03,	-6.5137043664457188e-03,	+6.7e-12
finite:	+1.9628928574388416e-02,	+1.9628928574411668e-02,	+1.2e-12

==== 0 --> u~ u g g g ====

	NJet:	Helac1loop:	rel.diff.
born:	+5.0328282104265365e-04,	+5.0328282104265484e-04,	+2.4e-15
1/eps^2:	-9.7283503961992726e-05,	-9.7283503961991818e-05,	+9.3e-15
1/eps:	-6.1775045952609201e-05,	-6.1775045952603048e-05,	+1.0e-13
finite:	+1.1409871173998674e-04,	+1.1409871173998645e-04,	+2.5e-15

==== 0 --> u~ u d~ d g ====

	NJet:	Helac1loop:	rel.diff.
born:	+3.6329475567709317e-04,	+3.6329475567709729e-04,	+1.1e-14
1/eps^2:	-5.0160076608990277e-05,	-5.0160076608990379e-05,	+2.0e-15
1/eps:	-4.1238301409751345e-05,	-4.1238301409752870e-05,	+3.7e-14
finite:	+1.6929367019718101e-05,	+1.6929367019719798e-05,	+1.0e-13

==== 0 --> u~ u u~ u g ====

	NJet:	Helac1loop:	rel.diff.
born:	+1.6607841328194570e-03,	+1.6607841328194737e-03,	+1.0e-14
1/eps^2:	-2.2930432666983780e-04,	-2.2930432666983907e-04,	+5.6e-15
1/eps:	-1.6167755068577280e-04,	-1.6167755068572718e-04,	+2.8e-13
finite:	+7.0356660045273211e-04,	+7.0356660045274610e-04,	+2.0e-14

----- 2 --> 4 -----

==== 0 --> u~ u g g g g ====

	NJet:	Helac1loop:	rel.diff.
born:	+2.4749786907729620e-05,	+2.4749786907729492e-05,	+5.2e-15
1/eps^2:	-6.0142737839968278e-06,	-6.0142737839968761e-06,	+8.0e-15
1/eps:	-1.4238548051572628e-05,	-1.4238548051576113e-05,	+2.4e-13
finite:	-2.1818575805881747e-06,	-2.1818575805944554e-06,	+2.9e-12

==== 0 --> u~ u d~ d g g ====

	NJet:	Helac1loop:	rel.diff.
born:	+3.8990501849846650e-06,	+3.8990501849846963e-06,	+8.0e-15
1/eps^2:	-7.3214448592467342e-07,	-7.3214448592467173e-07,	+2.3e-15
1/eps:	-1.5000972850719066e-06,	-1.5000972850719574e-06,	+3.4e-14
finite:	+1.1570207960122947e-07,	+1.1570207960076906e-07,	+4.0e-12

==== 0 --> u~ u u~ u g g ====

	NJet:	Helac1loop:	rel.diff.
born:	+1.2029972817541046e-05,	+1.2029972817541090e-05,	+3.7e-15
1/eps^2:	-2.2589291869350247e-06,	-2.2589291869350408e-06,	+7.1e-15
1/eps:	-4.9249280446345875e-06,	-4.9249280446538397e-06,	+3.9e-12



finite: +3.6301807851586739e-06, +3.6301807851561252e-06, +7.0e-13

==== 0 -->  $u \bar{u} d \bar{d} s \bar{s}$  ====

	NJet:	Helac1loop:	rel.diff.
born:	+4.6602437519749336e-08,	+4.6602437519749931e-08,	+1.3e-14
1/eps^2:	-6.1770188741857187e-09,	-6.1770188741856584e-09,	+9.8e-15
1/eps:	-1.2079244035518674e-08,	-1.2079244035518879e-08,	+1.7e-14
finite:	+3.0749739659342438e-09,	+3.0749739659321969e-09,	+6.7e-13

==== 0 -->  $u \bar{u} d \bar{d} d \bar{d}$  ====

	NJet:	Helac1loop:	rel.diff.
born:	+1.7752256666856891e-08,	+1.7752256666857116e-08,	+1.3e-14
1/eps^2:	-2.3530104931548807e-09,	-2.3530104931548365e-09,	+1.9e-14
1/eps:	-4.8669803368255748e-09,	-4.8669803368265401e-09,	+2.0e-13
finite:	+1.2351513905489450e-09,	+1.2351513905470286e-09,	+1.6e-12

==== 0 -->  $u \bar{u} u \bar{u} u \bar{u}$  ====

	NJet:	Helac1loop:	rel.diff.
born:	+1.9800262627817160e-06,	+1.9800262627817295e-06,	+6.8e-15
1/eps^2:	-2.6244677848455005e-07,	-2.6244677848455651e-07,	+2.5e-14
1/eps:	-3.5478617113255096e-07,	-3.5478617113278930e-07,	+6.7e-13
finite:	+1.2984349868781561e-06,	+1.2984349868773965e-06,	+5.8e-13

## B Numerical evaluation for 7-parton virtual corrections

We evaluate all indepenent channels contributing to the virtual corrections to  $pp \rightarrow 5$  jets at the following phase space point:

$$\begin{aligned}
p_1 &= \{-5.000000000000000 \times 10^2, 0.000000000000000 \times 10^0, \\
&\quad 0.000000000000000 \times 10^0, -5.000000000000000 \times 10^2\}, \\
p_2 &= \{-5.000000000000000 \times 10^2, 0.000000000000000 \times 10^0, \\
&\quad 0.000000000000000 \times 10^0, 5.000000000000000 \times 10^2\}, \\
p_3 &= \{8.6354068143781365 \times 10^1, -1.5213389320261800 \times 10^1, \\
&\quad 3.7633551294916273 \times 10^1, -7.6218722682185415 \times 10^1\}, \\
p_4 &= \{2.8011818180937634 \times 10^2, -8.3126111650582232 \times 10^1, \\
&\quad -2.6320385675865049 \times 10^2, 4.7749085116026578 \times 10^1\}, \\
p_5 &= \{1.2752252956966052 \times 10^2, -9.0449041295993482 \times 10^1, \\
&\quad -8.3178307703078929 \times 10^1, 3.4093043339258053 \times 10^1\}, \\
p_6 &= \{4.1413006837454346 \times 10^2, 2.3214556494593859 \times 10^2, \\
&\quad 3.3275443678081871 \times 10^2, -8.2985751852442578 \times 10^1\}, \\
p_7 &= \{9.1875152102638314 \times 10^1, -4.3357022679101075 \times 10^1, \\
&\quad -2.4005823614005564 \times 10^1, 7.7362346079343363 \times 10^1\}.
\end{aligned} \tag{B.1}$$

The result has been obtained with the number of light quark flavour  $n_f = 5$ , a renormalization scale of  $\mu_R = 91.188$  and  $\alpha_s = 0.118$ . Table 6 shows the numerical values of the amplitudes.

## References

- [1] S. Badger, B. Biedermann, and P. Uwer, *NGluon: A Package to Calculate One-loop Multi-gluon Amplitudes*, *Comput.Phys.Commun.* **182** (2011) 1674–1692, [[arXiv:1011.2900](#)].
- [2] S. Badger, B. Biedermann, P. Uwer, and V. Yundin, *NLO QCD corrections to multi-jet production at the LHC with a centre-of-mass energy of  $\sqrt{s} = 8$  TeV*, [arXiv:1209.xxxx](#).
- [3] Z. Bern, L. J. Dixon, D. C. Dunbar, and D. A. Kosower, *One loop n point gauge theory amplitudes, unitarity and collinear limits*, *Nucl.Phys.* **B425** (1994) 217–260, [[hep-ph/9403226](#)].
- [4] Z. Bern, L. J. Dixon, D. C. Dunbar, and D. A. Kosower, *Fusing gauge theory tree amplitudes into loop amplitudes*, *Nucl.Phys.* **B435** (1995) 59–101, [[hep-ph/9409265](#)].
- [5] R. Britto, F. Cachazo, and B. Feng, *Generalized unitarity and one-loop amplitudes in N=4 super-Yang-Mills*, *Nucl.Phys.* **B725** (2005) 275–305, [[hep-th/0412103](#)].
- [6] R. Ellis, W. Giele, and Z. Kunszt, *A Numerical Unitarity Formalism for Evaluating One-Loop Amplitudes*, *JHEP* **0803** (2008) 003, [[arXiv:0708.2398](#)].
- [7] W. T. Giele, Z. Kunszt, and K. Melnikov, *Full one-loop amplitudes from tree amplitudes*, *JHEP* **0804** (2008) 049, [[arXiv:0801.2237](#)].
- [8] D. Forde, *Direct extraction of one-loop integral coefficients*, *Phys.Rev.* **D75** (2007) 125019, [[arXiv:0704.1835](#)].

Channel	Born	2Re(Loop · Born)
$0 \rightarrow 7g$	$6.6739867626785 \times 10^{-7}$	$-2.6321266028904 \times 10^{-7} \cdot \epsilon^{-2}$ $1.2781291277818 \times 10^{-7} \cdot \epsilon^{-1}$ $-4.0556181173518 \times 10^{-7} \cdot \epsilon^0$
$0 \rightarrow \bar{u}u + 5g$	$8.2213902805466 \times 10^{-9}$	$-2.7277340128627 \times 10^{-9} \cdot \epsilon^{-2}$ $-4.6877933000518 \times 10^{-11} \cdot \epsilon^{-1}$ $-4.8319141582166 \times 10^{-9} \cdot \epsilon^0$
$0 \rightarrow \bar{u}u\bar{d}d + 3g$	$2.5689441485779 \times 10^{-9}$	$-6.9151881689636 \times 10^{-10} \cdot \epsilon^{-2}$ $7.9158077535594 \times 10^{-11} \cdot \epsilon^{-1}$ $-1.9006336322439 \times 10^{-9} \cdot \epsilon^0$
$0 \rightarrow \bar{u}u\bar{u}u + 3g$	$4.5631774024631 \times 10^{-9}$	$-1.2283346215940 \times 10^{-9} \cdot \epsilon^{-2}$ $4.9063178156336 \times 10^{-11} \cdot \epsilon^{-1}$ $-1.9994502250899 \times 10^{-9} \cdot \epsilon^0$
$0 \rightarrow \bar{u}u\bar{d}d\bar{s}s + g$	$2.8701338670235 \times 10^{-11}$	$-5.9292119796938 \times 10^{-12} \cdot \epsilon^{-2}$ $5.8421068466114 \times 10^{-13} \cdot \epsilon^{-1}$ $-1.5312833372355 \times 10^{-11} \cdot \epsilon^0$
$0 \rightarrow \bar{u}u\bar{d}d\bar{d}d + g$	$1.2779583891422 \times 10^{-11}$	$-2.6400462631767 \times 10^{-12} \cdot \epsilon^{-2}$ $-4.5891042883903 \times 10^{-13} \cdot \epsilon^{-1}$ $-6.6633865124667 \times 10^{-12} \cdot \epsilon^0$
$0 \rightarrow \bar{u}u\bar{u}u\bar{u}u + g$	$1.9091768148671 \times 10^{-9}$	$-3.9440369566465 \times 10^{-10} \cdot \epsilon^{-2}$ $1.9659510267642 \times 10^{-10} \cdot \epsilon^{-1}$ $-3.6659249528662 \times 10^{-10} \cdot \epsilon^0$

**Table 6.** The numerical evaluation of 7 parton virtual corrections at the phase space point given in eq. (B.1). Using  $\alpha_s = 0.118$ ,  $\mu_R = 91.188$  and including final state symmetry factors.

- [9] G. Ossola, C. G. Papadopoulos, and R. Pittau, *Reducing full one-loop amplitudes to scalar integrals at the integrand level*, *Nucl.Phys.* **B763** (2007) 147–169, [[hep-ph/0609007](#)].
- [10] F. Cascioli, P. Maierhofer, and S. Pozzorini, *Scattering Amplitudes with Open Loops*, *Phys.Rev.Lett.* **108** (2012) 111601, [[arXiv:1111.5206](#)].
- [11] G. Ossola, C. G. Papadopoulos, and R. Pittau, *CutTools: A Program implementing the OPP reduction method to compute one-loop amplitudes*, *JHEP* **0803** (2008) 042, [[arXiv:0711.3596](#)].
- [12] W. Giele and G. Zanderighi, *On the Numerical Evaluation of One-Loop Amplitudes: The Gluonic Case*, *JHEP* **0806** (2008) 038, [[arXiv:0805.2152](#)].
- [13] C. Berger, Z. Bern, L. Dixon, F. Febres Cordero, D. Forde, *et. al.*, *An Automated Implementation of On-Shell Methods for One-Loop Amplitudes*, *Phys.Rev.* **D78** (2008) 036003, [[arXiv:0803.4180](#)].
- [14] P. Mastrolia, G. Ossola, T. Reiter, and F. Tramontano, *Scattering AMplitudes from Unitarity-based Reduction Algorithm at the Integrand-level*, *JHEP* **1008** (2010) 080, [[arXiv:1006.0710](#)].
- [15] V. Hirschi, R. Frederix, S. Frixione, M. V. Garzelli, F. Maltoni, *et. al.*, *Automation of one-loop QCD corrections*, *JHEP* **1105** (2011) 044, [[arXiv:1103.0621](#)].
- [16] G. Cullen, N. Greiner, G. Heinrich, G. Luisoni, P. Mastrolia, *et. al.*, *Automated One-Loop Calculations with GoSam*, *Eur.Phys.J.* **C72** (2012) 1889, [[arXiv:1111.2034](#)].

- [17] J. M. Campbell and R. K. Ellis,  $t\bar{t}W^{+-}$  production and decay at NLO, *JHEP* **1207** (2012) 052, [[arXiv:1204.5678](#)].
- [18] S. Badger, J. M. Campbell, and R. Ellis, QCD corrections to the hadronic production of a heavy quark pair and a W-boson including decay correlations, *JHEP* **1103** (2011) 027, [[arXiv:1011.6647](#)].
- [19] S. Badger, R. Sattler, and V. Yundin, One-Loop Helicity Amplitudes for  $t\bar{t}$  Production at Hadron Colliders, *Phys.Rev.* **D83** (2011) 074020, [[arXiv:1101.5947](#)].
- [20] J. M. Campbell and R. K. Ellis, Top-quark processes at NLO in production and decay, [arXiv:1204.1513](#).
- [21] J. M. Campbell, R. K. Ellis, and C. Williams, Hadronic production of a Higgs boson and two jets at next-to-leading order, *Phys.Rev.* **D81** (2010) 074023, [[arXiv:1001.4495](#)].
- [22] J. M. Campbell, R. K. Ellis, and C. Williams, Gluon-Gluon Contributions to  $W^+ W^-$  Production and Higgs Interference Effects, *JHEP* **1110** (2011) 005, [[arXiv:1107.5569](#)].
- [23] C. Berger, Z. Bern, L. J. Dixon, F. Febres Cordero, D. Forde, *et. al.*, Precise Predictions for  $W + 3$  Jet Production at Hadron Colliders, *Phys.Rev.Lett.* **102** (2009) 222001, [[arXiv:0902.2760](#)].
- [24] C. Berger, Z. Bern, L. J. Dixon, F. Febres Cordero, D. Forde, *et. al.*, Next-to-Leading Order QCD Predictions for  $W+3$ -Jet Distributions at Hadron Colliders, *Phys.Rev.* **D80** (2009) 074036, [[arXiv:0907.1984](#)].
- [25] C. Berger, Z. Bern, L. J. Dixon, F. Febres Cordero, D. Forde, *et. al.*, Next-to-Leading Order QCD Predictions for  $Z, \gamma^*+3$ -Jet Distributions at the Tevatron, *Phys.Rev.* **D82** (2010) 074002, [[arXiv:1004.1659](#)].
- [26] A. Bredenstein, A. Denner, S. Dittmaier, and S. Pozzorini, NLO QCD corrections to  $pp \rightarrow t$  anti- $t$   $b$  anti- $b + X$  at the LHC, *Phys.Rev.Lett.* **103** (2009) 012002, [[arXiv:0905.0110](#)].
- [27] A. Bredenstein, A. Denner, S. Dittmaier, and S. Pozzorini, NLO QCD Corrections to Top Anti-Top Bottom Anti-Bottom Production at the LHC: 2. full hadronic results, *JHEP* **1003** (2010) 021, [[arXiv:1001.4006](#)].
- [28] G. Bevilacqua, M. Czakon, C. Papadopoulos, R. Pittau, and M. Worek, Assault on the NLO Wishlist:  $\rightarrow t$  anti- $t$   $b$  anti- $b$ , *JHEP* **0909** (2009) 109, [[arXiv:0907.4723](#)].
- [29] F. Campanario, C. Englert, M. Rauch, and D. Zeppenfeld, Precise predictions for  $W \gamma \gamma + \text{jet}$  production at hadron colliders, *Phys.Lett.* **B704** (2011) 515–519, [[arXiv:1106.4009](#)].
- [30] G. Bevilacqua, M. Czakon, C. Papadopoulos, and M. Worek, Dominant QCD Backgrounds in Higgs Boson Analyses at the LHC: A Study of  $pp \rightarrow t$  anti- $t + 2$  jets at Next-To-Leading Order, *Phys.Rev.Lett.* **104** (2010) 162002, [[arXiv:1002.4009](#)].
- [31] A. Denner, S. Dittmaier, S. Kallweit, and S. Pozzorini, NLO QCD corrections to  $WWbb$  production at hadron colliders, *Phys.Rev.Lett.* **106** (2011) 052001, [[arXiv:1012.3975](#)].
- [32] G. Bevilacqua, M. Czakon, A. van Hameren, C. G. Papadopoulos, and M. Worek, Complete off-shell effects in top quark pair hadroproduction with leptonic decay at next-to-leading order, *JHEP* **1102** (2011) 083, [[arXiv:1012.4230](#)].
- [33] G. Bevilacqua, M. Czakon, C. Papadopoulos, and M. Worek, Hadronic top-quark pair production in association with two jets at Next-to-Leading Order QCD, *Phys.Rev.* **D84** (2011) 114017, [[arXiv:1108.2851](#)].
- [34] A. Denner, S. Dittmaier, S. Kallweit, and S. Pozzorini, NLO QCD corrections to off-shell top-antitop production with leptonic decays at hadron colliders, [arXiv:1207.5018](#).

- [35] G. Bevilacqua and M. Worek, *Constraining BSM Physics at the LHC: Four top final states with NLO accuracy in perturbative QCD*, *JHEP* **1207** (2012) 111, [[arXiv:1206.3064](#)].
- [36] T. Binoth, N. Greiner, A. Guffanti, J. Reuter, J.-P. Guillet, *et. al.*, *Next-to-leading order QCD corrections to  $pp \rightarrow b \text{ anti-}b b \text{ anti-}b + X$  at the LHC: the quark induced case*, *Phys.Lett.* **B685** (2010) 293–296, [[arXiv:0910.4379](#)].
- [37] N. Greiner, A. Guffanti, T. Reiter, and J. Reuter, *NLO QCD corrections to the production of two bottom-antibottom pairs at the LHC*, *Phys.Rev.Lett.* **107** (2011) 102002, [[arXiv:1105.3624](#)].
- [38] N. Greiner, G. Heinrich, P. Mastrolia, G. Ossola, T. Reiter, *et. al.*, *NLO QCD corrections to the production of  $W^+ W^-$  plus two jets at the LHC*, *Phys.Lett.* **B713** (2012) 277–283, [[arXiv:1202.6004](#)].
- [39] K. Melnikov and G. Zanderighi,  *$W+3$  jet production at the LHC as a signal or background*, *Phys.Rev.* **D81** (2010) 074025, [[arXiv:0910.3671](#)].
- [40] R. K. Ellis, K. Melnikov, and G. Zanderighi,  *$W+3$  jet production at the Tevatron*, *Phys.Rev.* **D80** (2009) 094002, [[arXiv:0906.1445](#)].
- [41] T. Melia, K. Melnikov, R. Rontsch, and G. Zanderighi, *NLO QCD corrections for  $W^+W^-$  pair production in association with two jets at hadron colliders*, *Phys.Rev.* **D83** (2011) 114043, [[arXiv:1104.2327](#)].
- [42] T. Melia, K. Melnikov, R. Rontsch, and G. Zanderighi, *Next-to-leading order QCD predictions for  $W^+W^+jj$  production at the LHC*, *JHEP* **1012** (2010) 053, [[arXiv:1007.5313](#)].
- [43] C. Berger, Z. Bern, L. J. Dixon, F. Febres Cordero, D. Forde, *et. al.*, *Precise Predictions for  $W + 4$  Jet Production at the Large Hadron Collider*, *Phys.Rev.Lett.* **106** (2011) 092001, [[arXiv:1009.2338](#)].
- [44] H. Ita, Z. Bern, L. Dixon, F. Febres Cordero, D. Kosower, *et. al.*, *Precise Predictions for  $Z + 4$  Jets at Hadron Colliders*, *Phys.Rev.* **D85** (2012) 031501, [[arXiv:1108.2229](#)].
- [45] R. Frederix, S. Frixione, K. Melnikov, and G. Zanderighi, *NLO QCD corrections to five-jet production at LEP and the extraction of  $\alpha_s(M_Z)$* , *JHEP* **1011** (2010) 050, [[arXiv:1008.5313](#)].
- [46] S. Becker, D. Goetz, C. Reuschle, C. Schwan, and S. Weinzierl, *NLO results for five, six and seven jets in electron-positron annihilation*, *Phys.Rev.Lett.* **108** (2012) 032005, [[arXiv:1111.1733](#)].
- [47] S. Frixione and B. R. Webber, *Matching NLO QCD computations and parton shower simulations*, *JHEP* **0206** (2002) 029, [[hep-ph/0204244](#)].
- [48] S. Frixione, P. Nason, and C. Oleari, *Matching NLO QCD computations with Parton Shower simulations: the POWHEG method*, *JHEP* **0711** (2007) 070, [[arXiv:0709.2092](#)].
- [49] S. Alioli, P. Nason, C. Oleari, and E. Re, *A general framework for implementing NLO calculations in shower Monte Carlo programs: the POWHEG BOX*, *JHEP* **1006** (2010) 043, [[arXiv:1002.2581](#)].
- [50] S. Alioli, K. Hamilton, P. Nason, C. Oleari, and E. Re, *Jet pair production in POWHEG*, *JHEP* **1104** (2011) 081, [[arXiv:1012.3380](#)].
- [51] M. Garzelli, A. Kardos, C. Papadopoulos, and Z. Trocsanyi,  *$Z0$  - boson production in association with a top anti-top pair at NLO accuracy with parton shower effects*, *Phys.Rev.* **D85** (2012) 074022, [[arXiv:1111.1444](#)].
- [52] M. Garzelli, A. Kardos, C. Papadopoulos, and Z. Trocsanyi, *Standard Model Higgs boson production in association with a top anti-top pair at NLO with parton showering*, *Europhys.Lett.* **96** (2011) 11001, [[arXiv:1108.0387](#)].

- [53] R. Frederix, S. Frixione, V. Hirschi, F. Maltoni, R. Pittau, *et. al.*, *Scalar and pseudoscalar Higgs production in association with a top-antitop pair*, *Phys.Lett.* **B701** (2011) 427–433, [[arXiv:1104.5613](#)].
- [54] R. Frederix, S. Frixione, V. Hirschi, F. Maltoni, R. Pittau, *et. al.*, *W and Z/ $\gamma^*$  boson production in association with a bottom-antibottom pair*, *JHEP* **1109** (2011) 061, [[arXiv:1106.6019](#)].
- [55] A. Kardos, Z. Trocsanyi, and C. Papadopoulos, *Top quark pair production in association with a Z-boson at NLO accuracy*, *Phys.Rev.* **D85** (2012) 054015, [[arXiv:1111.0610](#)].
- [56] A. Kardos, C. Papadopoulos, and Z. Trocsanyi, *Top quark pair production in association with a jet with NLO parton showering*, *Phys.Lett.* **B705** (2011) 76–81, [[arXiv:1101.2672](#)].
- [57] S. Alioli, S.-O. Moch, and P. Uwer, *Hadronic top-quark pair-production with one jet and parton showering*, *JHEP* **1201** (2012) 137, [[arXiv:1110.5251](#)].
- [58] J. M. Campbell, R. K. Ellis, R. Frederix, P. Nason, C. Oleari, *et. al.*, *NLO Higgs boson production plus one and two jets using the POWHEG BOX, MadGraph4 and MCFM*, *JHEP* **1207** (2012) 092, [[arXiv:1202.5475](#)].
- [59] S. Hoeche, F. Krauss, M. Schonherr, and F. Siegert, *W+n-jet predictions with MC@NLO in Sherpa*, *Physical Review Letters* (2012) [[arXiv:1201.5882](#)].
- [60] W. Giele, Z. Kunszt, and J. Winter, *Efficient Color-Dressed Calculation of Virtual Corrections*, *Nucl.Phys.* **B840** (2010) 214–270, [[arXiv:0911.1962](#)].
- [61] S. Becker, C. Reuschle, and S. Weinzierl, *Efficiency improvements for the numerical computation of NLO corrections*, *JHEP* **1207** (2012) 090, [[arXiv:1205.2096](#)].
- [62] T. Binoth, F. Boudjema, G. Dissertori, A. Lazopoulos, A. Denner, *et. al.*, *A Proposal for a standard interface between Monte Carlo tools and one-loop programs*, *Comput.Phys.Commun.* **181** (2010) 1612–1622, [[arXiv:1001.1307](#)]. Dedicated to the memory of, and in tribute to, Thomas Binoth, who led the effort to develop this proposal for Les Houches 2009.
- [63] G. van Oldenborgh, *FF: A Package to evaluate one loop Feynman diagrams*, *Comput.Phys.Commun.* **66** (1991) 1–15.
- [64] R. K. Ellis and G. Zanderighi, *Scalar one-loop integrals for QCD*, *JHEP* **0802** (2008) 002, [[arXiv:0712.1851](#)].
- [65] A. van Hameren, *OneLoop: For the evaluation of one-loop scalar functions*, *Comput.Phys.Commun.* **182** (2011) 2427–2438, [[arXiv:1007.4716](#)].
- [66] S. Badger, B. Biedermann, and P. Uwer, *Numerical evaluation of one-loop QCD amplitudes*, *Journal of Physics: Conference Series* **368** (2012) 012055, [[arXiv:1112.0412](#)].
- [67] S. Badger, B. Biedermann, and P. Uwer, *One-Loop Amplitudes for Multi-Jet Production at Hadron Colliders*, [arXiv:1201.1187](#). 8 pages, 5 figures, 2 tables. Talk given at RADCOR 2011, Mamallapuram, India, 26 - 30 September, 2011.
- [68] Z. Bern, L. J. Dixon, and D. A. Kosower, *One loop corrections to two quark three gluon amplitudes*, *Nucl.Phys.* **B437** (1995) 259–304, [[hep-ph/9409393](#)].
- [69] R. Ellis, Z. Kunszt, K. Melnikov, and G. Zanderighi, *One-loop calculations in quantum field theory: from Feynman diagrams to unitarity cuts*, [arXiv:1105.4319](#).
- [70] F. A. Berends and W. T. Giele, *Recursive Calculations for Processes with n Gluons*, *Nucl. Phys.* **B306** (1988) 759.



- [71] Z. Bern and A. Morgan, *Massive loop amplitudes from unitarity*, *Nucl.Phys.* **B467** (1996) 479–509, [[hep-ph/9511336](#)].
- [72] Z. Bern, L. J. Dixon, D. C. Dunbar, and D. A. Kosower, *One loop selfdual and  $N=4$  superYang-Mills*, *Phys.Lett.* **B394** (1997) 105–115, [[hep-th/9611127](#)].
- [73] Z. Bern and D. A. Kosower, *The Computation of loop amplitudes in gauge theories*, *Nucl.Phys.* **B379** (1992) 451–561.
- [74] S. Badger, *Direct Extraction Of One Loop Rational Terms*, *JHEP* **0901** (2009) 049, [[arXiv:0806.4600](#)].
- [75] C. F. Berger and D. Forde, *Multi-Parton Scattering Amplitudes via On-Shell Methods*, *Ann.Rev.Nucl.Part.Sci.* **60** (2010) 181–205, [[arXiv:0912.3534](#)].
- [76] R. Ellis, W. Giele, Z. Kunszt, K. Melnikov, and G. Zanderighi, *One-loop amplitudes for  $W^+$  3 jet production in hadron collisions*, *JHEP* **0901** (2009) 012, [[arXiv:0810.2762](#)].
- [77] H. Ita and K. Ozeren, *Colour Decompositions of Multi-quark One-loop QCD Amplitudes*, *JHEP* **1202** (2012) 118, [[arXiv:1111.4193](#)].
- [78] L. J. Dixon, *Calculating scattering amplitudes efficiently*, [hep-ph/9601359](#).
- [79] R. K. Ellis, K. Melnikov, and G. Zanderighi, *Generalized unitarity at work: first NLO QCD results for hadronic  $W^+$  3jet production*, *JHEP* **0904** (2009) 077, [[arXiv:0901.4101](#)].
- [80] S. Catani and M. Seymour, *The Dipole formalism for the calculation of QCD jet cross-sections at next-to-leading order*, *Phys.Lett.* **B378** (1996) 287–301, [[hep-ph/9602277](#)].
- [81] S. Catani, S. Dittmaier, and Z. Trocsanyi, *One loop singular behavior of QCD and SUSY QCD amplitudes with massive partons*, *Phys.Lett.* **B500** (2001) 149–160, [[hep-ph/0011222](#)].
- [82] Y. Hida, X. S. Li, and D. H. Bailey. <http://crd.lbl.gov/~dhbailey/mpdist/>, 2010.
- [83] **Particle Data Group** Collaboration, G. Yost *et. al.*, *Review of Particle Properties: Particle Data Group*, *Phys.Lett.* **B204** (1988) 1–486.
- [84] R. K. Ellis and J. Sexton, *QCD Radiative Corrections to Parton Parton Scattering*, *Nucl.Phys.* **B269** (1986) 445.
- [85] Z. Bern, L. J. Dixon, and D. A. Kosower, *One loop corrections to five gluon amplitudes*, *Phys.Rev.Lett.* **70** (1993) 2677–2680, [[hep-ph/9302280](#)].
- [86] Z. Bern, L. J. Dixon, and D. A. Kosower, *On-shell recurrence relations for one-loop QCD amplitudes*, *Phys.Rev.* **D71** (2005) 105013, [[hep-th/0501240](#)].
- [87] D. Forde and D. A. Kosower, *All-multiplicity one-loop corrections to MHV amplitudes in QCD*, *Phys.Rev.* **D73** (2006) 061701, [[hep-ph/0509358](#)].
- [88] Z. Bern, L. J. Dixon, and D. A. Kosower, *The last of the finite loop amplitudes in QCD*, *Phys.Rev.* **D72** (2005) 125003, [[hep-ph/0505055](#)]. 45 pages, revtex, 7 figures, v2 minor corrections Report-no: SLAC-PUB-11134, UCLA/05/TEP/15, Saclay/SPhT-T05/058 Journal-ref: Phys.Rev. D72 (2005) 125003.
- [89] Z. Bern, G. Diana, L. Dixon, F. Febres Cordero, S. Hoeche, *et. al.*, *Four-Jet Production at the Large Hadron Collider at Next-to-Leading Order in QCD*, [arXiv:1112.3940](#).
- [90] G. Bevilacqua, M. Czakon, M. Garzelli, A. van Hameren, A. Kardos, *et. al.*, *HELAC-NLO*, [arXiv:1110.1499](#).
- [91] E. Byckling and K. Kajantie, *Particle kinematics*. Wiley, 1973.